

PHYSICAL SCIENCES

Molecular “surgery” on a 23-gold-atom nanoparticle

Qi Li,^{1*} Tian-Yi Luo,^{2*} Michael G. Taylor,^{3*} Shuxin Wang,^{1†} Xiaofan Zhu,¹ Yongbo Song,¹ Giannis Mpourmpakis,³ Nathaniel L. Rosi,² Rongchao Jin^{1‡}

¹Department of Chemistry, Carnegie Mellon University, Pittsburgh, PA 15213, USA.

²Department of Chemistry, University of Pittsburgh, Pittsburgh, PA 15260, USA.

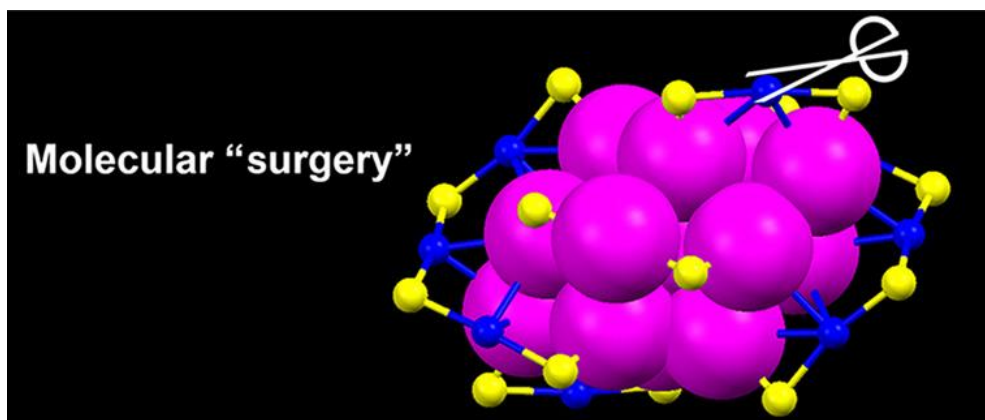
³Department of Chemical Engineering, University of Pittsburgh, Pittsburgh, PA 15261, USA.

‡Corresponding author. Email: rongchao@andrew.cmu.edu

* These authors contributed equally to this work.

† Present address: Department of Chemistry, Anhui University Hefei, Anhui 230601, China.

Science Advances 19 May 2017:
Vol. 3, no. 5, e1603193
DOI: 10.1126/sciadv.1603193



Esma Khatun
29/07/17

Introduction

- In recent years, major advancement have been achieved in the synthesis of Au, Ag, and Au/Ag alloy nanoclusters. Exploring effective methods to exquisitely tailor the size, structure, and composition of atomically precise nanoclusters constitutes an ultimate goal in this field, which will offer opportunities to pursue fundamental understanding of the properties of nanoclusters and establish definitive structure-property relationships.
- Numerous effective methodologies that can precisely tailor specific groups in organic molecules without altering the major carbon bones have been developed, but for nanoparticles, it is still extremely difficult to realize the atomic-level tailoring of specific sites in a particle without changing the structure of other parts.
- This issue severely limits nanochemists from knowing how different motifs in a nanoparticle contribute to its overall properties.

In this paper...

- They demonstrated a site-specific “surgery” on the surface motif of $[\text{Au}_{23}(\text{SR})_{16}]^-$ nanoparticle by a two-step metal-exchange method, which led to the “resection” of two surface gold atoms and the formation of a new 21-gold-atom nanoparticle, $[\text{Au}_{21}(\text{SR})_{12}(\text{Ph}_2\text{PCH}_2\text{PPh}_2)_2]^+$, without changing the other parts of the starting nanoparticle structure.
- This precise surgery of the nanoclusters revealed the different reactivity of the surface motifs and the inner core: the least effect of surface motifs on optical absorption but a distinct effect on photoluminescence.
- First-principles calculations further reveal the thermodynamically preferred reaction pathway for the formation of $[\text{Au}_{21}(\text{SR})_{12}(\text{Ph}_2\text{PCH}_2\text{PPh}_2)_2]^+$.

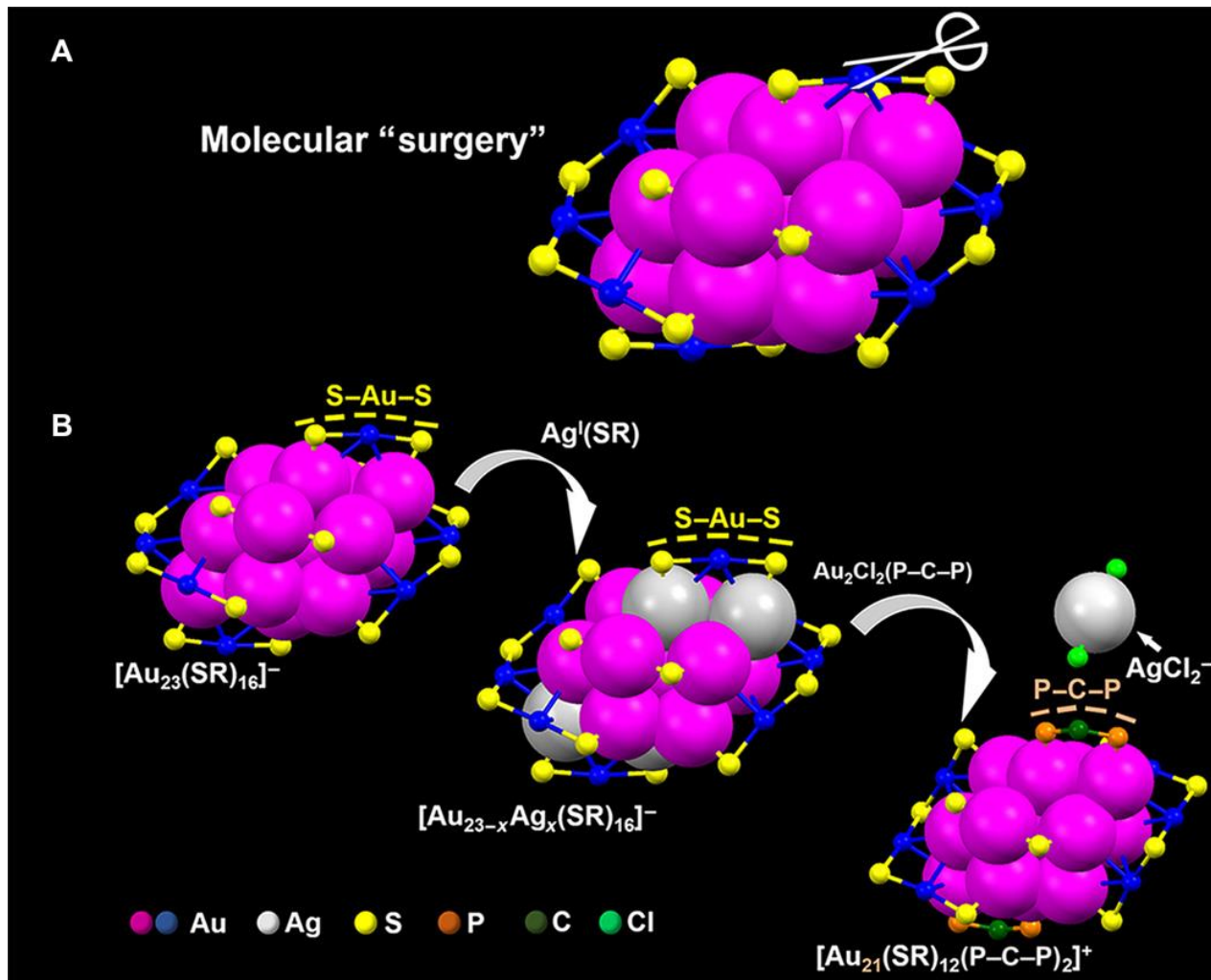


Fig. 1. Molecular surgery on the atomically precise 23-gold-atom nanocluster by a two-step metal-exchange method: peeling off two parts of the cluster wrapper and closing the gaps with two P–C–P plasters. (A) Schematic of the molecular surgery on $[Au_{23}(SR)_{16}]^{-}$; all carbon tails are omitted for clarity. (B) Site-specific surface motif tailoring with a two-step metal-exchange method. The transformation from $[Au_{23}(SR)_{16}]^{-}$ through $[Au_{23-x}Ag_x(SR)_{16}]^{-}$ ($x \sim 1$) to $[Au_{21}(SR)_{12}(P-C-P)_2]^{+}$ is revealed by single-crystal x-ray analysis. Magenta and blue, Au; gray, Ag; yellow, S; orange, P; green, C; light green, Cl. Other C and all H atoms are omitted for clarity.

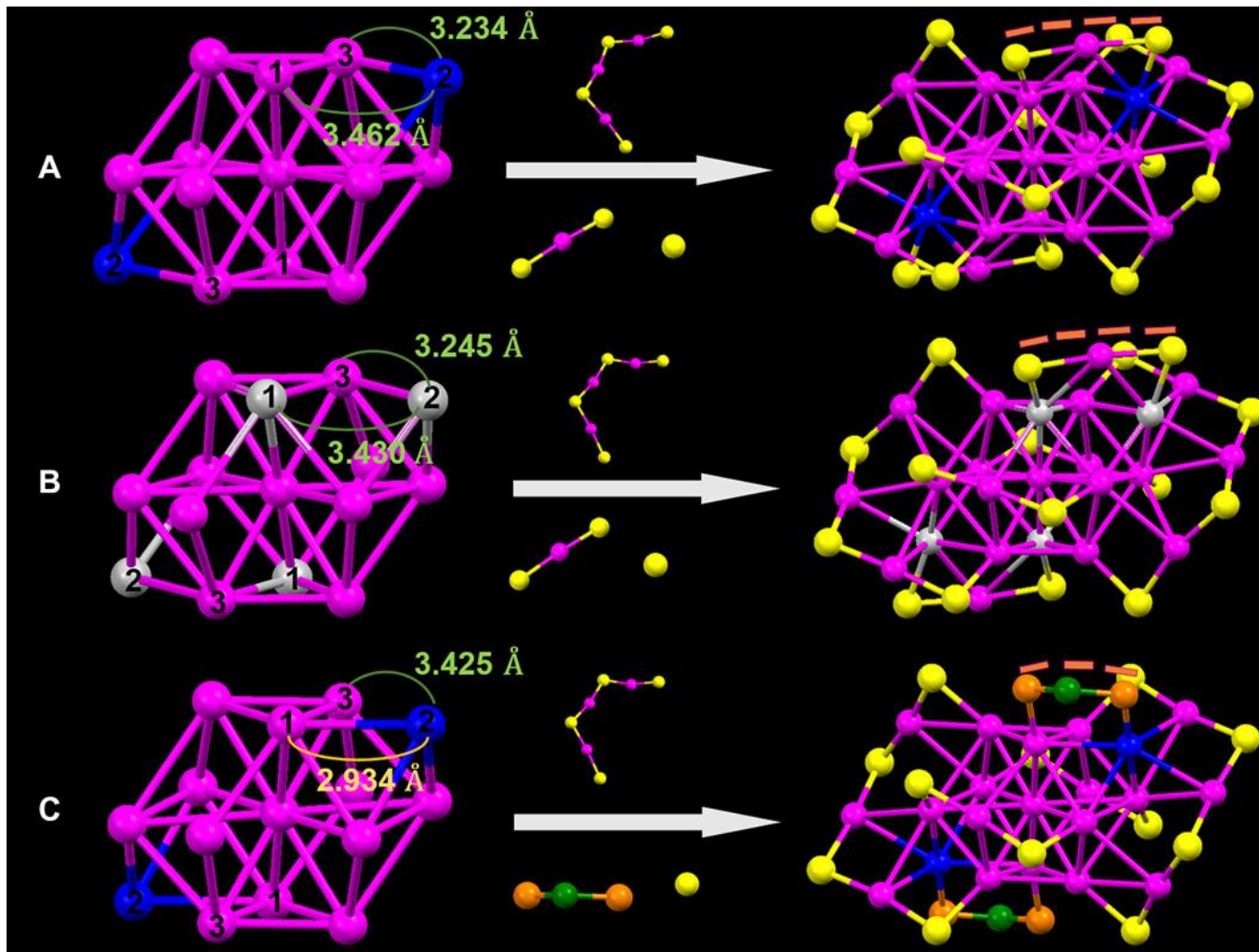


Fig. 2. Comparison of the $[\text{Au}_{23}(\text{SR})_{16}]^{-}$, $[\text{Au}_{23-x}\text{Ag}_x(\text{SR})_{16}]^{-}$, and $[\text{Au}_{21}(\text{SR})_{12}(\text{P-C-P})_2]^{+}$ structures. (A) Crystal structure of $[\text{Au}_{23}(\text{SR})_{16}]^{-}$. Left: 15-atom Au bipyramidal core. Right: $\text{Au}_{23}\text{S}_{16}$ framework. (B) Crystal structure of $[\text{Au}_{23-x}\text{Ag}_x(\text{SR})_{16}]^{-}$. Left: 15-atom Au-Ag bipyramidal core. Right: $\text{Au}_{23-x}\text{Ag}_x\text{S}_{16}$ framework. (C) Crystal structure of $[\text{Au}_{21}(\text{SR})_{12}(\text{P-C-P})_2]^{+}$. Left: 15-atom bipyramidal core. Right: $\text{Au}_{21}\text{S}_{12}(\text{P-C-P})_2$ framework. Magenta and blue, Au; gray, Ag; yellow, S; orange, P; green, C. Other C and all H atoms are omitted for clarity. The counterions TOA^{+} and AgCl_2^{-} are also omitted.

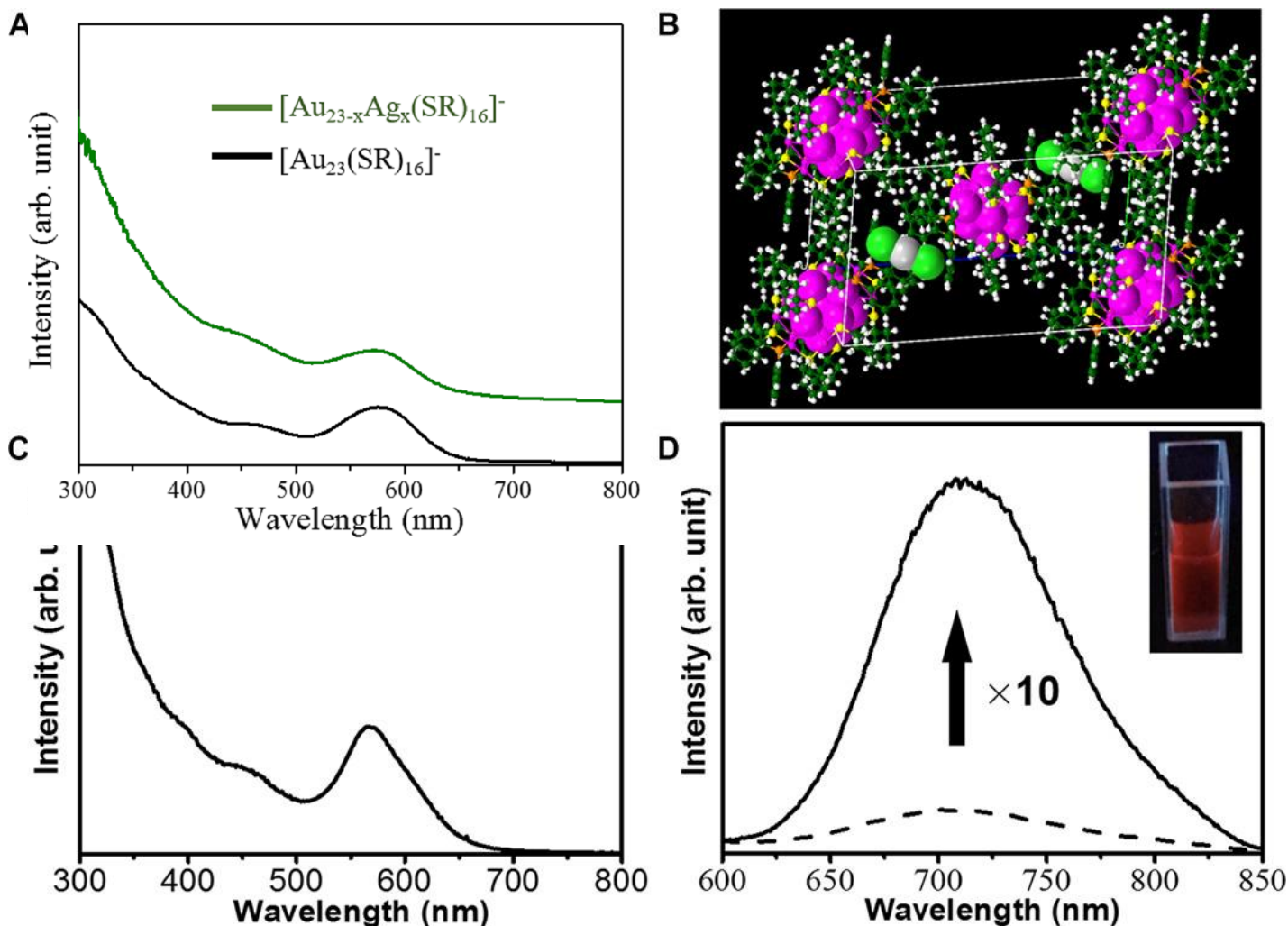
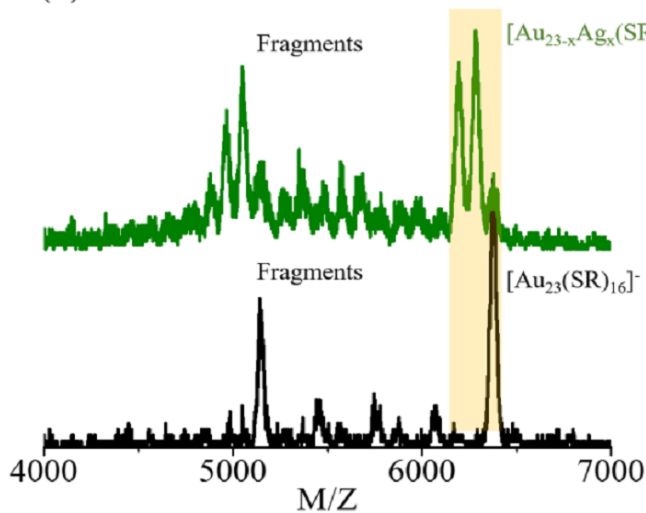


Fig. 3. Single-crystal structure and optical properties of $[\text{Au}_{21}(\text{SR})_{12}(\text{P-C-P})_2]^+[\text{AgCl}_2]^-$. (A) The counter anion $[\text{AgCl}_2]^-$ and coordination of $\text{PPh}_2\text{CH}_2\text{PPh}_2$ motifs. Other carbon tails and all H atoms are removed for clarity. (B) Total structure and arrangement of $[\text{Au}_{21}(\text{SR})_{12}(\text{P-C-P})_2]^+[\text{AgCl}_2]^-$ in a single-crystal unit cell. Magenta, Au; gray, Ag; yellow, S; orange, P; green, C; light green, Cl; white, H. (C) UV-Vis absorption spectrum of $[\text{Au}_{21}(\text{SR})_{12}(\text{P-C-P})_2]^+$. (D) PL spectrum of the Au_{21} (solid line); the PL efficiency is enhanced ~ 10 times compared to Au_{23} (dashed line). Inset shows a photograph of the Au_{21} sample under 365-nm UV light.

(a)



(b)

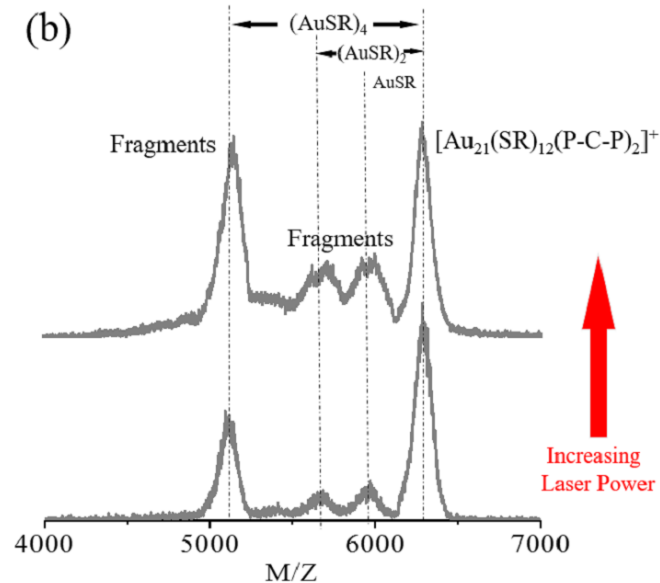
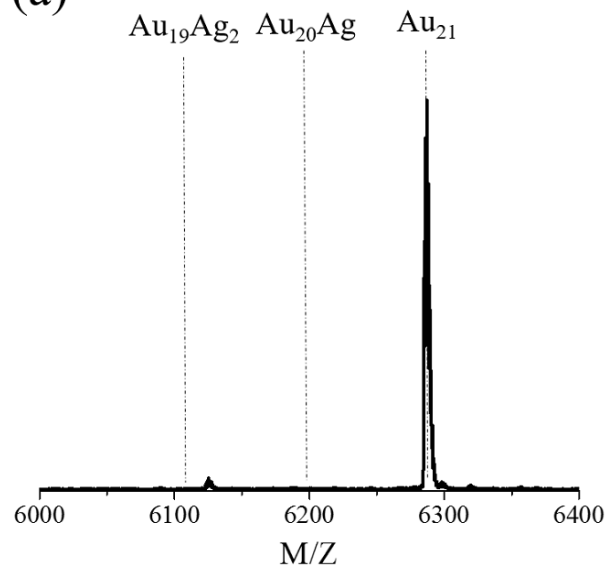


fig. S2. MALDI mass spectra of $[\text{Au}_{23}(\text{SR})_{16}]^-$ (black), $[\text{Au}_{23-x}\text{Ag}_x(\text{SR})_{16}]^-$ (green), and $[\text{Au}_{21}(\text{SR})_{12}(\text{P-C-P})_2]^+$ (gray) sample.

(a)



(b)

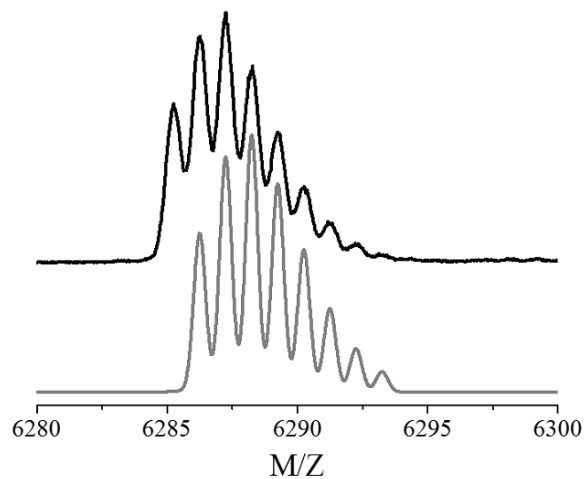


fig. S3. ESI mass spectrum of $[\text{Au}_{21}(\text{SR})_{12}(\text{P-C-P})_2]^+$

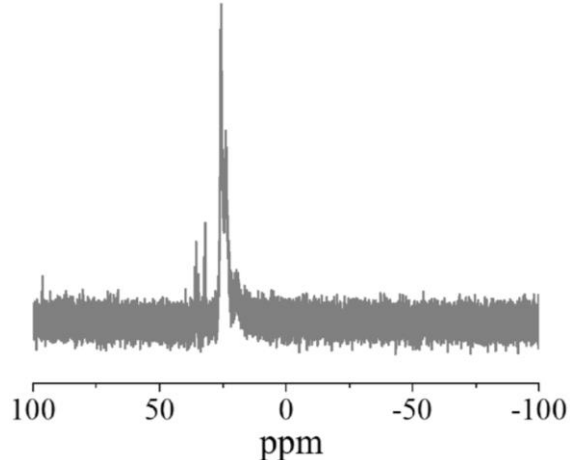


fig. S4. ^{31}P -NMR spectrum of $[\text{Au}_{21}(\text{SR})_{12}(\text{P-C-P})_2]^+$

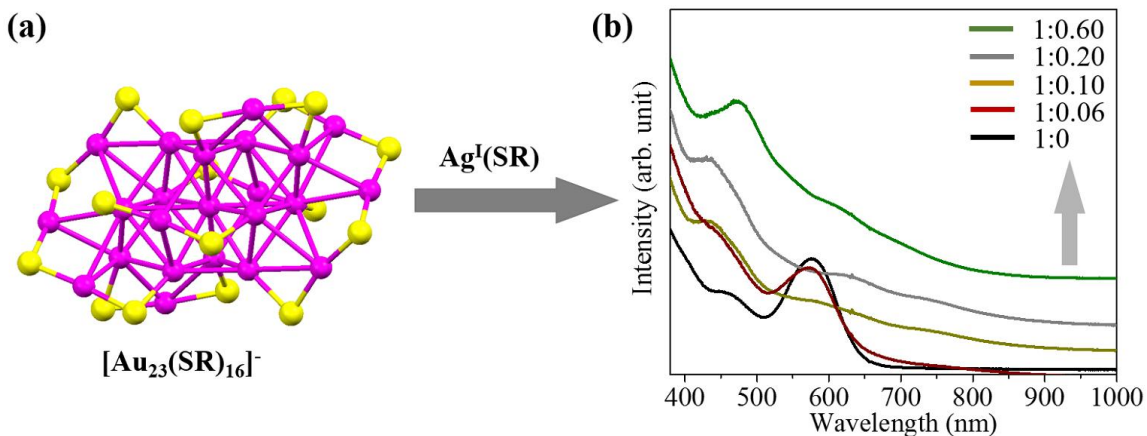


fig. S5. UV-Vis absorption spectra of samples with increasing mass ratio of $\text{Ag}^{\text{I}}(\text{SR})$ that reacted with $[\text{Au}_{23}(\text{SR})_{16}]^-$

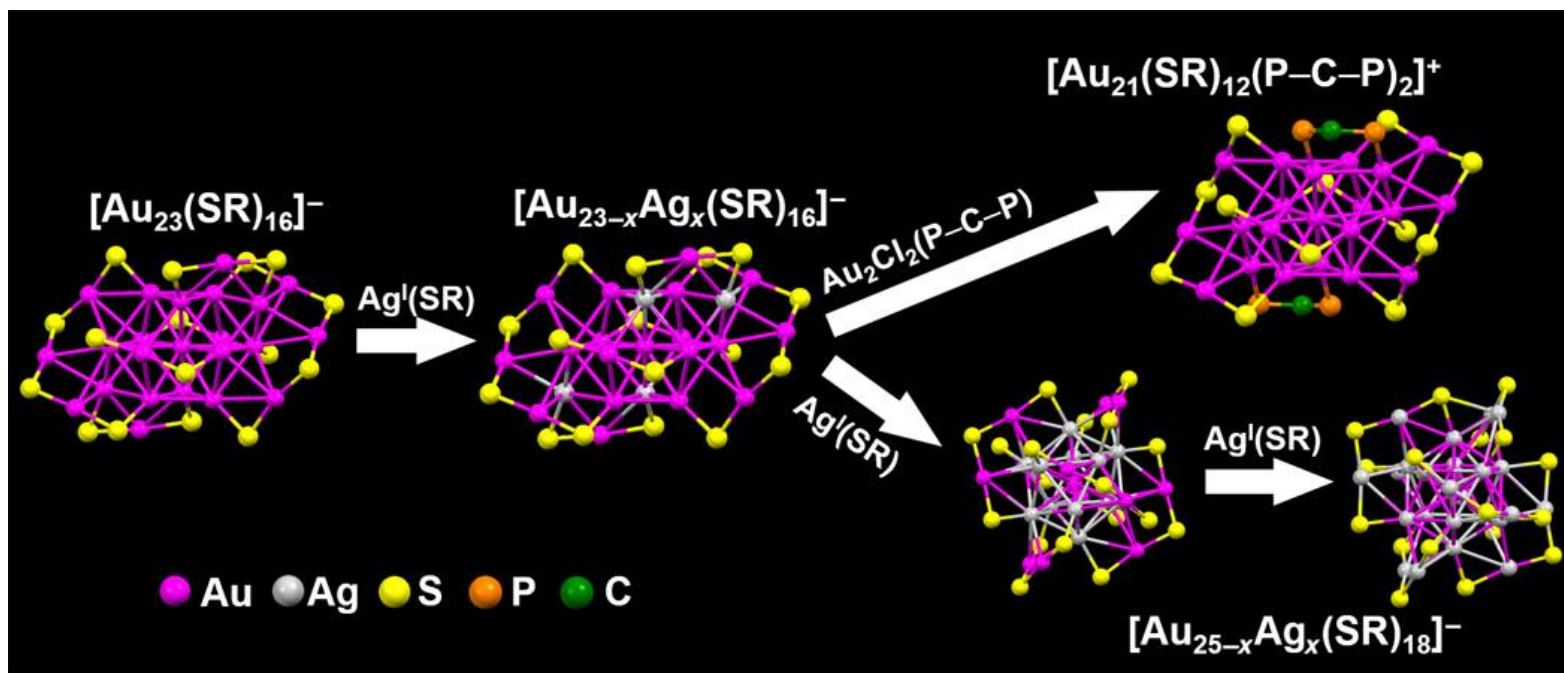


Fig. 4. Metal-exchange transformation from $[\text{Au}_{23}(\text{SR})_{16}]^-$ to $[\text{Au}_{21}(\text{SR})_{12}(\text{P-C-P})_2]^+$ and $[\text{Au}_{25-x}\text{Ag}_x(\text{SR})_{18}]^-$.

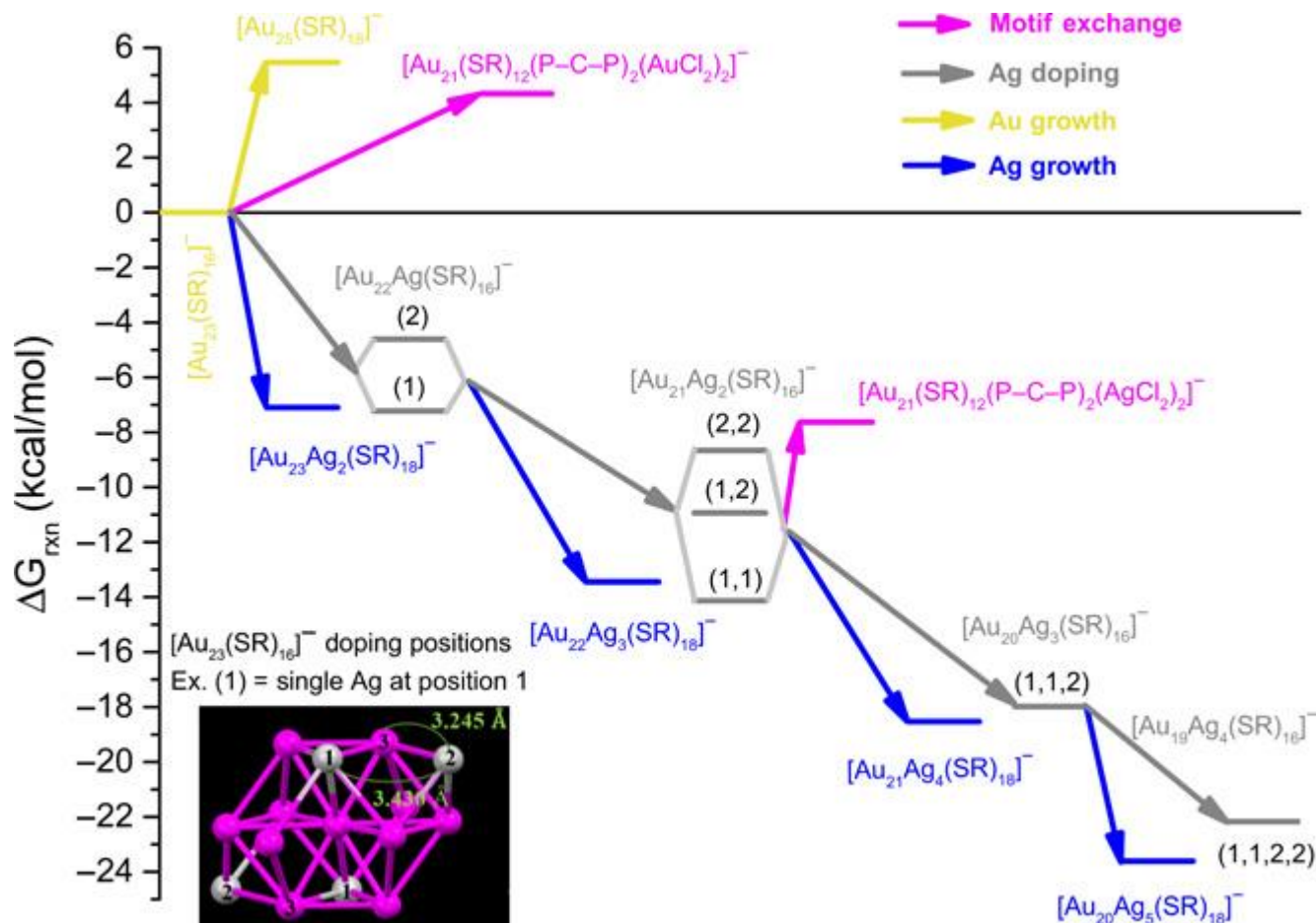


Fig. 5. DFT-calculated free energies (ΔG_{rxn}) of elementary reaction steps of the experimentally synthesized pure and Ag-doped Au nanoclusters. Detailed reaction network energetics analysis can be found in table S4. Inset shows the different (thermodynamically stable) doping positions of Ag in the Au_{15} core of the $[\text{Au}_{23-x}\text{Ag}_x(\text{SR})_{16}]^-$ clusters. The different energy levels of the $[\text{Au}_{23-x}\text{Ag}_x(\text{SR})_{16}]^-$ clusters represent the lowest-energy isomers (based on doping positions of the inset), which are also analysed in fig. S8.

Conclusion

- A two-step metal-exchange method was developed for site-specific surface motif exchange on $[\text{Au}_{23}(\text{SR})_{16}]^-$ to form a new $[\text{Au}_{21}(\text{SR})_{12}(\text{P}-\text{C}-\text{P})_2]^+$ nanocluster.
- Both experimental and DFT calculations indicate that the formation of the $[\text{Au}_{23-x}\text{Ag}_x(\text{SR})_{16}]^-$ ($x=1$ to 2) intermediate is critical, and the dopant Ag atoms are target-doped at two specific positions (partial occupancy).
- Doping lowers the transformation barrier and thus enables transformation from Au₂₃ to Au₂₁ when $[\text{Au}_{23-x}\text{Ag}_x(\text{SR})_{16}]^-$ reacts with $\text{Au}_2\text{Cl}_2(\text{P}-\text{C}-\text{P})$, whereas the reaction with more $\text{Ag}^+(\text{SR})$ leads to size/structure changes and the formation of $\text{Au}_{25-x}\text{Ag}_x$.
- This work offers a promising strategy for molecular surgery on nanoclusters to tailor their structure and functionality.